Vacancy-Formation Energy and Entropy in Magnesium Single Crystals

C. Janot, D. Mallėjac, and B. George
Laboratoire de Physique du Solide, Ensmim, Parc de Saurupt 54, *Nancy, France*
(Received 26 March 1970)

Macroscopic thermal dilatation coefficients as well as those of the lattice have been precisely measured along principal crystallographic directions of magnesium single crystals in the temperature range between room temperature and 650 °C. The vacancy concentration was thus obtained as a function of temperature and it reached the value of 72×10^{-5} in the neighborhood of the melting point. An appreciable anisotropy in the atom rearrangement appears during the defect-formation process, which seems to correspond to a preferential climb of edge dislocations in the prismatic planes. From the behavior of the excess in macroscopic dilatation as a function of temperature, the formation energy is found to be 0.58 eV per vacancy, while the formation entropy is practically zero.

I. INTRODUCTION

The volume of a perfect crystal at low temperatures can be written as

$$V_0 = N_0\Omega_0 ,$$

where Ω_0 is the atomic volume which is constant throughout the lattice and N_0 is the number of lattice sites or the number of atoms. Raising the temperature results in both a uniform dilatation of the atomic volume due to the lattice-vibration anharmonicity and the appearance of point defects. The latter modifies the total number of lattice sites and produces a relaxation effect which modifies the mean atomic volume. Then, it is necessary to define a new atomic volume Ω for N sites in the equilibrium temperature T; the volume of the crystal can be written as

$$V = N\Omega .$$

For a reversible increase in temperature dT from T,

$$dV/V = dN/N + d\Omega/\Omega .$$

If it is supposed that the macroscopic-dilatation tensors and those of the lattice, although different, have superposed principal axes, it is possible to describe the relative increase of the number of sites as a function of both the macroscopic relative dilatation and that of the lattice,

$$\frac{dN}{N} = \sum_{i=1}^{3} \frac{dL_i}{L_i} - \frac{da_i}{a_i} \quad . \tag{1}$$

The coefficients dL_i/L_i can be macroscopically determined while da_i/a_i can be found by diffractometric observations since the lattice appears with an atomic density and, therefore, an electronic density which is a triply periodic function showing well-defined maxima.

Calculation shows that, for a precision of 10^{-5} on the increase of the number of sites relative to a state of reference without defects, an integration of Eq. (1) is required. One obtains

$$\ln\left(\frac{N}{N_0}\right) = \sum_{i=1}^{3} \ln\left(\frac{L_i}{L_{0i}}\right) - \ln\left(\frac{a_i}{a_{0i}}\right) ,$$

and the concentration is given by (for a precision of 10^{-5})

$$c = \sum_{i=1}^{3} \ln\left(1+\frac{\Delta L_i}{L_{0i}}\right) - \ln\left(1+\frac{\Delta a_i}{a_{0i}}\right) \quad . \tag{2}$$

One obtains the well-known first-order development result of Eshelby's[1] calculation which was used mainly by Simmons and Balluffi to obtain the formation energies and entropies of vacancies in aluminium,[2] silver,[3] gold,[4] and copper[5] from simultaneous measurements of specimen widths and lattice parameters. For these different materials, as well as for lead[6] and sodium,[7] the structure is cubic; therefore, the defect concentration can be obtained from only one series of measurements on the same specimen.

For an hexagonal crystal, however, the c axis is different from the two equivalent basal axes. The relation (2) is then written as

$$c = \ln(1+\Delta L_{\parallel}/L_0) - \ln(1+\Delta a_{\parallel}/a_0) + 2[\ln(1+\Delta L_{\perp}/L_0) - \ln(1+\Delta a_{\perp}/a_0)] . \tag{3}$$

The indices $\parallel$ and $\perp$ refer to the directions parallel and perpendicular to the c axis, respectively. A first-order development gives the relation used by Feder and Nowick for cadmium.[8] In this case, single crystals must be used and two series of measurements must be made to determine the dilatation coefficients for the principal directions.

II. EXPERIMENTAL METHODS

A. Specimen Preparation

The specimens were of two types: single-crystal bars 500 mm in length for the macroscopic dilatation studies and small single-crystal plates for the lattice-dilatation observations. Single crystals having diameters of about 4 cm were grown by the Bridgman technique using vertical graphite crucibles with pointed lower ends. The speed of the melted zone travel was 2 mm/h. The single crystals were placed in a goniometric support and cut with a spark cutter to obtain oriented single-crystal plates for lattice observations.

Seeds were also cut and used for the growth of very large single crystals in the form of parallelepiped bars. The method consists in placing the seed, a few centimeters in length and 1 cm^2 in cross section, in the desired orientation beside a 600-mm-long magnesium bar of the same cross section and containing 100 ppm of impurities. A melted zone which partially melts the seed and welds it to the Mg bar is made to travel to the other end, thus imposing the seed's orientation on the bar. The specimens selected were those forming 7° and 77° between the growth axis and the c axis. Their monocrystalline nature was verified by a series of Laue photographs. The initially irregular faces of the bars were spark polished to eliminate the presence of external stresses during the dilatation measurements. The perturbed superficial layer was removed with diluted nitric acid and the specimens were rinsed with alcohol and doubly distilled water. Elongation measurements were made using tungsten reference points stuck vertically on holes about 500 mm apart bored on one face of the bar. This is found to be the best method, considering the amount of evaporation of Mg in the neighborhood of its melting point.

The platelet preparation for the lattice-parameter measurements is much simpler. Considering the geometry of the heating system, they were made in such a way as to fit against a face of the bar and present a plane towards the exterior for the diffractometer measurements.

B. Measurement Apparatus

The system was described and used by Bianchi[9] and Mallejac.[10] The specimen, entirely enclosed in a 180-cm graphite piece provided with observation windows, is placed in the refractory steel tube (70 mm diam) of the 3.5-m-long furnace. The furnace has five independent windings and the temperature is made constant in time and space by a system of regulation; the temperature measurement uses a single thermocouple which travels 1 mm above and parallel to the specimen. Thus, it was possible to maintain a constant temperature throughout the length of the bars for more than 30 min and more than 4 h at the x-ray observation windows with an accuracy of 0.1°.

To avoid pollution and evaporization of Mg, the study was made in an atmosphere of purified helium at a pressure of 3 bars.

The macroscopic elongation measurements were made with an optical dilatometer consisting essentially of two microscopes equipped with cross hairs and a system of image transfer. They are fixed rigidly with bars of Invar at controlled temperatures. The successive sighting of the reference points is done by moving the assembly with the use of a micrometer which reads 0.1 μ. Preliminary adjustments are realized with three translations and one rotation of the assembly.

For the lattice-dilatation measurements, a modified "rotating crystal method" was used in which the crystal is fixed and the diffractometer oscillates around an axis contained in the plane of the platelets. A 1-m optical lever allows a reading of the order of 10^{-5} for the relative displacement of the diffraction spot corresponding to the selective reflection chosen. Since the entry and exit of the x rays in the furnace is limited by a 30° cone, the reflections of the $K\alpha_1$ of Fe on the planes $(01\bar{1}5)$ and $K\alpha_1$ of Co on the planes $(12\bar{3}3)$ were used.

C. Measurements

After annealing for several days in the neighborhood of 450 °C, a bar and a platelet were subjected to successive temperature increases at 20° intervals from room temperature to the neighborhood of the melting point in such a way as to be able to trace simultaneously the macroscopic- and microscopic-dilatation curves on two neighboring crystallographic directions. This process is repeated several times before another set of specimens is observed.

1. *Principal Macroscopic Dilatations*

The measurements give directly the relative dilatations $\Delta L_{(1)}/L$ and $\Delta L_{(2)}/L$ for the two bars having axes forming 7° and 77° angles with th axis, respectively.

Table I gives an example of the experimental results obtained in a late series of measurements for $\Delta L_{(1)}/L$ and $\Delta L_{(2)}/L$.

The dilatation on the principal crystallographic directions is therefore the result of a combination of the two series of independent measurements. This combination is not linear since the dilatation anisotropy produces a change in the angles between the characteristic directions of the structure. A more rigorous calculation gives

$$\frac{\Delta L_\perp}{L_0}=\left(1+\frac{\sin^2\alpha_1[2\Delta L_{(2)}/L_0+(\Delta L_{(2)}/L_0)^2]-\sin^2\alpha_2[2\,\Delta L_{(1)}/L_0+(\Delta L_{(1)}/L_0)^2]}{\sin(\alpha_1+\alpha_2)\sin(\alpha_1-\alpha_2)}\right)^{1/2}-1\,,$$

$$\frac{\Delta L_\parallel}{L_0}=\left(1+\frac{\cos^2\alpha_2[2\Delta L_{(1)}/L_0+(\Delta L_{(1)}/L_0)^2]-\cos^2\alpha_1[2\,\Delta L_{(2)}/L_0+(\Delta L_{(2)}/L_0)^2]}{\sin(\alpha_1+\alpha_2)\sin(\alpha_1-\alpha_2)}\right)^{1/2}-1\,, \tag{4}$$

where α_1 and α_2 are, respectively, the angles formed by the measurement directions with the basal plane; $\Delta L_{(1)}/L_0$ and $\Delta L_{(2)}/L_0$ having been determined at different temperatures, the experimental values are replaced by two fourth-degree polynomials whose coefficients have been found by computer calculations. One can also replace the polynomials by a parabolic interpolation.

2. *Principal Lattice Dilatations*

Knowing perfectly the diffractometer geometry, one can deduce, in the same manner outlined above, the principal lattice dilatations from the measured values. An error calculation shows immediately the impossibility of determining this geometry to an accuracy of 10^{-6}–10^{-5} using classical methods. One must be contented with an accuracy of 10^{-2}–10^{-3} and a precise mathematical determination which identifies the macroscopic dilatations with those of the lattice for a given direction at low temperatures where the point defect concentration is not detectable. The calculation is as follows: One calculates the lattice distances $d(T)$ as a function of temperature up to about 400 °C for the family of planes $(01\bar{1}5)$ and $(12\bar{3}3)$ by the relation

$$d(T)^2=\frac{3a^2}{4}\,\frac{1}{h^2+k^2+hk+\frac{3}{4}(a^2/c^2)\,l^2}\,, \tag{5}$$

where

$$a=a_0(1+\Delta a/a_0)=a_0(1+\Delta L_\perp/L_0)\,,$$
$$c=c_0(1+\Delta c/c_0=c_0(1+\Delta L_\parallel/L_0)\,.$$

From this, one deduces the values of the corresponding Bragg angles

$$\theta(T)=\arcsin(\lambda/2d(T))\,. \tag{6}$$

These values $\theta(T)$ are adjusted mathematically, using a computer, to those obtained from the geometry of the system (Fig. 1):

$$\theta(T)=\arcsin\frac{\lambda}{2d(T)}\equiv\frac{\pi}{2}-\frac{1}{2}\arctan\frac{\{[h\cos\phi+(X-b)\sin\phi]^2-(e-e_0)^2\}^{1/2}}{h\sin\phi-(X-b)\cos\phi}\,, \tag{7}$$

where h is the distance between the specimen and the photographic plate JH, b is the distance between the reference point O on the film to the foot on the

TABLE I. Experimental values for $\Delta L_{(1)}/L_0$ and $\Delta L_{(2)}/L_0$ after macroscopic stabilization of the specimens.

T (°C)	$10^5\Delta L_{(1)}/L_0$	T (°C)	$10^5\Delta L_{(2)}/L_0$
17.9	−19.9	56.8	79.4
48.6	62.8	74.7	124.2
73.5	130.7	102.2	197.7
117.3	255.4	127.8	267.3
144.2	331.6	169.8	383.2
179.0	432.6	205.7	485.2
213.0	533.3	232.8	564.2
244.8	629.0	259.7	643.5
310.7	834.3	304.2	779.5
333.4	906.1	341.0	893.1
367.6	1015.5	363.6	964.0
389.5	1087.1	394.8	1065.5
408.7	1149.0	413.7	1126.8
431.1	1223.8	437.8	1206.9
446.6	1275.2	457.2	1272.3
468.5	1351.0	492.6	1394.6
496.7	1449.1	521.2	1497.1
534.7	1581.4	556.9	1631.2
566.1	1695.6	591.2	1763.9
591.0	1787.0	612.8	1850.0
613.3	1872.2	635.4	1941.6
634.0	1951.3	646.0	1985.6
647.7	2012.3		

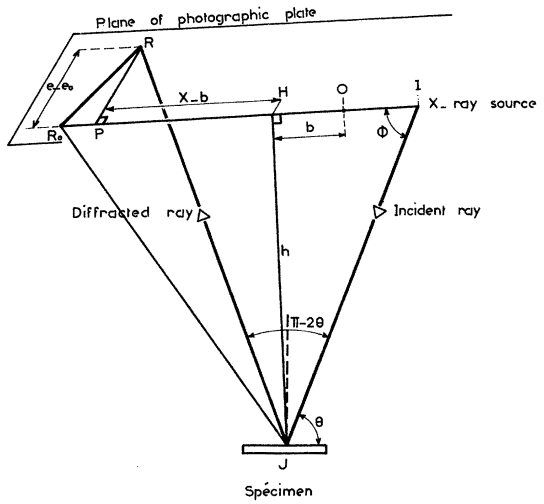

FIG. 1. Diffractometer geometry. Symbols are defined in the text.

plate of the perpendicular to the specimen OH, ϕ is the angle between the horizontal projection of the plate and the incident rays, $X(T)$ is the coordinate OP of the diffraction spot referred to the reference point O, $e - e_0$ is the height of the average diffracted ray referred to the horizontal plane containing the average incident ray, and $X(T)$ are the experimentally obtained quantities; the other values result from the mathematical adjustment.

Knowing the diffractometer geometry, one calculates for $\theta_1(T)$ and $\theta_2(T)$ up to the melting point using experimental values [Eq. (7)]. From these, one obtains $d_1(T)$ and $d_2(T)$ [Eq. (6)] and finally the principal lattice dilatations $\Delta a_\perp/a_0$ and $\Delta a_\parallel/a_0$ [Eq. (5)] for the whole range of temperatures.

Again, a series of independent measurements at various temperatures are involved in the calculations, thus making the use of a polynomial adjustment or a parabolic interpolation necessary for each series of measurements.

3. *Formation Energy and Entropy*

Using Eq. (3), it is possible to calculate the point defect concentration $c(T)$ as a function of temperature. Finally, these values $c(T)$ are identified with those given by the relation

$$c(T) = A\, e^{-E_f/kT} . \tag{8}$$

Usually, the quantity $\ln c$ is adjusted to a function in $(1/T)$. In this case, the greater uncertainty for the points at low temperatures would correspond to a smaller statistical weight. It is preferable to determine directly A and E_f by the method of least squares for the minimum of

$$W = \sum_i [c(T_i) - A\, e^{-E_f/kT_i}]^2 .$$

The calculation[9] shows that it is obtained for the maximum value of

$$\rho^2(E_f) = (\sum_i u_i y_i)^2 / \sum_i u_i^2 \sum_i y_i^2 \quad ,$$

where

$$y_i = c(T_i), \quad u_i = e^{-E_f/kT_i} .$$

The energy of formation E_f^* is then given by the abscissa corresponding to the maximum of the curve $\rho^2(E_f)$ which is obtained by a computer calculation. The entropy coefficient A^* is then estimated by

$$A^* = \sum_i y_i u_i / \sum_i u_i^2 , \quad \text{when } E_f = E_f^* .$$

A confidence range on the values of A and E_f can be determined by the following conditions:

$$(A - A_0)(n-2)^{1/2} = \{[\sum_i (u_i^2 - V_i^2) - (\sum_i u_i V_i)^2] / [\sum_i y_i^2 \sum_i V_i^2 - (\sum_i y_i V_i)^2]\}^{1/2} ,$$

$$(E - E_0)(A/k)(n-2)^{1/2} = \{[\sum_i u_i^2 \sum_i V_i^2 - (\sum_i u_i V_i)^2] / [\sum_i y_i^2 \sum_i u_i^2 - (\sum_i y_i u_i)^2]\} ,$$

after the law of Student for $n-2$ degrees of freedom, where n is the number of points taken into consideration and

$$V_i = u_i / T_i .$$

This calculated confidence range takes into account only the uncertainty due to the scatter in the experimental measurements and holds only for the assumption of a single type of thermal defect. In this sense, it is an optimistic estimate of the true error in the energy and entropy of formation. Systematic errors which may have an appreciable effect on the results are not included. However, it would seem that such systematic errors, if they exist, would make it very difficult, if not impossible, to obtain reasonable values for h, b, and ϕ, which are adjusted mathematically by identifying the macroscopic dilatations with those of the lattice at low temperatures.

III. EXPERIMENTAL RESULTS

A. Macroscopic Measurements

During the raising or lowering of the temperature, the regularity of the dilatation curves can be followed by tracing the changes in length as a function of temperature on diagrams of large dimensions (7 m×4 m). The curves do not superpose for the first heating-cooling cycles; a residual dilatation appears at room temperature. Two successive heatings on the same specimen give very different curves at low temperatures (up to 500 °C for the direction near the basal plane and 300 °C for the direction near the c axis) which converge towards each other at higher temperatures to coincide perfectly at temperatures near the melting point. After three or four heating-cooling cycles, this phenomenon disappears and the macroscopic dilatation curves coincide within the precision of the experiment.

Table II gives the values of $\Delta L/L_0$ for the two measurement directions corresponding to the first and last raising of temperature. The differences between the initial and final dilatation coefficients illustrate the analysis described. The values given in Table II result from a polynomial adjustment of the experimental values, and their less than 10^{-5} spread shows that the desired accuracy is attained.

B. Lattice Measurements

Here, the experimental quantities are the positions $X(T)$ of the diffraction spots. It has been stated above how the diffractometer geometry must first be determined from macroscopic measure-

TABLE II. Values of $\Delta L/L_0$ for the two measurement directions corresponding to the first and last raising of temperature.

T (°C)	$10^5\Delta L/L_0$ near basal plane		$10^5\Delta L/L_0$ near c axis		$10^5C'$
	First temp. rise	Last temp. rise	First temp. rise	Last temp. rise	
25	0	0	0	0	0
50	64.3	62.2	70.3	67.2	9.2
75	130.1	126.3	141.8	135.7	14.8
100	197.4	192.0	214.0	205.5	19.5
125	266.1	259.4	287.2	276.5	23.7
150	336.1	328.1	361.1	348.5	27.6
175	407.2	398.2	435.9	421.6	30.7
200	479.6	469.4	511.3	495.6	35.9
225	553.0	541.9	587.5	570.6	37.0
250	627.6	615.5	664.5	646.5	41.8
275	703.2	690.3	742.1	723.2	42.5
300	780.0	766.2	820.5	800.9	45.3
325	858.0	843.2	899.7	879.4	48.9
350	937.2	921.5	979.7	959.0	51.9
375	1017.7	1001.1	1060.6	1039.5	55.8
400	1099.6	1082.1	1142.5	1121.0	59.8
425	1183.0	1164.5	1225.4	1203.7	64.5
450	1268.0	1248.6	1309.4	1287.6	69.9
475	1354.7	1334.5	1394.6	1372.9	75.4
500	1443.4	1422.4	1481.1	1459.5	81.6
525	1534.1	1512.5	1569.1	1547.7	88.4
550	1627.2	1604.9	1658.7	1637.7	96.4
575	1722.8	1700.0	1750.0	1729.6	104.3
600	1821.0	1798.0	1843.2	1823.5	113.9
625	1922.3	1899.1	1938.4	1919.7	124.6
650	2026.8	2003.8	2035.9	2018.2	135.6

ments using Eqs. (5)–(7).

The initial estimation of the geometric elements by direct measurements are within an accuracy of 10^{-2}–10^{-3}; for instance, the distance between the photographic plate and the specimen, h, is known within an accuracy of 1 mm. The difference between the estimated and the adjusted [Eq. (7)] values is called "Δh correction." It appears that the first series of parameter measurements $X_i(T)$ cannot be adjusted by Eq. (7) to the angle $\theta(T)$ calculated from the first macroscopic-dilatation measurements at low temperatures; the "correction Δh" must be of the order of 10 mm, which is not acceptable. On the other hand, if the measurements corresponding to the last heating-cooling cycles are used, the adjustment gives only a correction Δh not exceeding 1 mm and which can decrease up to 0.1 mm for certain $X_i(T)$ series.

Analogous observations were made concerning the "corrections" Δb, $\Delta\phi$, and $\Delta(e-e_0)$ on the geometric parameters b, ϕ, and $(e-e_0)$ which were directly determined for each series of measurements.

As long as the macroscopic dilatation curves do not superpose, they cannot be used for the equilibrium point-defect concentration determinations. It must be noted that the described initial process is involved only in the macroscopic-dilatation coefficients and does not affect the lattice dilatation.

C. Formation Energy and Entropy

The adjustment of Eq. (8) was done by making use of the following experimental results: (i) macroscopic and lattice measurements on only the last two series. The mathematical adjustment was done by parabolic interpolation between groups of three experimental points. This gives $E_f = 0.59$ eV and $A = 1.186$; (ii) the same measurements as (i) but using the polynomial adjustment $E_f = 0.57$ eV and $A = 0.932$; (iii) all measurements except for the nonreproducible measurements of the first cycle, $E_f = 0.58 \pm 0.01$ eV, $A = 1.05$, or $S_f = (0 \pm 0.3)k$. Table III shows the results which led to these determinations. The quantities

$$\delta_\perp = \frac{\Delta L_\perp}{L_0} - \frac{\Delta a_\perp}{a_0} \quad \text{and} \quad \delta_\parallel = \frac{\Delta L_\parallel}{L_0} - \frac{\Delta a_\parallel}{a_0}$$

characterize the influence of the appearance of

TABLE III. General results after a polynomial adjustment.

T (°C)	$10^5\delta_\perp$	$10^5\delta_\parallel$	10^5C
30	0.9	1.2	2.7
50	1.0	0.3	1.9
70	0.9	−0.3	1.1
90	0.8	−0.7	0.6
110	0.6	−0.9	0.0
130	0.3	−1.0	−0.7
150	0.0	−0.9	−1.0
170	−0.4	−0.7	−1.6
190	−0.6	−0.5	−1.7
210	−0.9	−0.3	−2.3
230	−1.0	0.0	−2.3
250	−1.1	0.1	−2.4
270	−1.2	0.3	−2.3
290	−1.1	0.5	−2.1
310	−1.0	0.5	−1.6
330	−0.6	0.6	−0.9
350	−0.2	0.5	−0.2
370	0.5	0.5	1.2
390	1.1	0.5	2.6
410	2.2	0.5	4.6
430	3.1	0.5	6.4
450	4.5	0.7	9.3
470	5.9	0.8	12.3
490	7.6	1.2	16.0
510	9.4	1.8	20.1
530	11.5	2.7	25.1
550	13.8	3.9	30.9
570	16.3	5.4	37.1
590	19.0	7.4	44.3
610	21.9	9.9	52.5
630	25.1	13.1	61.8
650	28.3	16.9	71.9
T_f 651	28.4	17.1	72.2

vacancies in the planes parallel and perpendicular to the basal plane, respectively. The ratio $\delta_\perp/\delta_\parallel$ is always greater than unity and is a decreasing function of temperature; it takes the value 7 near 480 °C and 1.7 near the melting point. The same type of observations were made on cadmium by Feder and Nowick[8] and on zinc by Gilder and Wallmark.[11]

IV. DISCUSSION AND INTERPRETATION OF RESULTS

A. Mechanism of Defect Formation

For convenience, the macroscopic measurements were made on two different monocrystalline specimens. In order that the two series of measurements be complementary, the defect effect should behave in the same manner on the two specimens following the principal crystallographic directions. This effect is dependent on the nature of the sources and sinks for vacancies: grain boundaries, which are not present in our single crystals; subboundaries, which can be viewed as dislocation structures; the surface, which depends on the form of the specimens. It is possible to show in the present case that the dislocations are responsible for the vacancy emission and trapping.

Taking, for example, the simple reasoning of Damask and Dienes,[12] the rate of vacancy creation (+ sign) and annihilation (− sign) can be written as $dn/dt = \pm \alpha D n$, where n is the number of point defects present at a given instant, D is the diffusion coefficient of the material, and α is a numerical factor depending on the nature of the sources or sinks. For the surfaces,

$$\alpha_s = \pi^2 (1/L_1^2 + 1/L_2^2 + 1/L_3^2)/\text{sites per cm}^2$$

if the specimen is a parallelepiped of dimensions L_1, L_2, L_3. In the present case, $\alpha_s \simeq 20/\text{sites per cm}^2$.

For a dislocation density N_0 per cm^2,

$$\alpha_D = 2N_0/\ln(r_1/r_0)\ ,$$

with

$$r_0 \simeq a_0 \quad \text{and} \quad \pi r_1^2 \simeq 1/N_0\ .$$

Here, the dislocation density is greater than 10^5/cm^2, hence

$$\alpha_D \geq 10^5/\text{sites per cm}^2\ .$$

Thus, the frequency of absorption and emission of vacancies is at least 5000 times greater on the dislocations than on the surfaces. The creation and annihilation of point defects occurs in the volume and the effect of the free surfaces is negligible.

This justifies the method used and one can understand the following two experimental observations.

1. *Anisotropy of Site Creation*

The ratio of the quantities $\delta_\perp$ and $\delta_\parallel$ shown in Table III is always greater than unity and decreases regularly with increasing temperature. This means that the excess atoms which appear after vacancy creation move preferentially in the prismatic planes and much more so for a low density of vacancies. The product of dislocation density and the velocity of dislocation climb is therefore larger for the prismatic plane than for the basal plane. On the other hand, the ratio $\delta_\perp/\delta_\parallel$ indicates that the velocity of climb increases much faster in the basal plane with increasing temperature. It is interesting to note that this anisotropy of site creation lowers the natural anisotropy of magnesium by decreasing macroscopic-dilatation anisotropy much faster than that of the lattice dilatation.

2. *Dilatation Anomaly for First Heating Cycles*

The measurements show a perfect reproducibility for the lattice dilatations but the same cannot be

said of the macroscopic dilatations. For a given direction, all the curves $\Delta L(T)$ coincide near the melting point, but at room temperature there is an appreciable spread of data for the first two or three heating cycles. When the low-temperature dilatation coefficients no longer change, there appears a relative residual dilatation of 23×10^{-5} for the direction forming 77° with the c axis and 17.7×10^{-5} for the direction forming 7° with the c axis. It is easy to eliminate the effect of creep since the specimens do not show any elongation when they are maintained for several days at a given temperature even in the neighborhood of the melting point. Neither can pollution of the specimen from the helium atmosphere, the graphite crucible, the Fe furnace tube, or traces of oxygen in the furnace explain this residual dilatation. The saturation of the phenomenon after two or three cycles would mean that the pollution is so much as to make the specimen a definite and stable alloy, which should considerably affect the lattice measurements; but no such effect was observed.

Finally, the possible instability of the tungsten reference points must be taken into account. However, it is difficult to understand why this instability would manifest itself several times at low temperatures (region of dilatation anomalies for the first cycles) and never at high temperatures (all the macroscopic-dilatation curves coincide at high temperatures).

The residual dilatation can be explained in terms of structural defect rearrangements. In the making of single-crystal specimens, a melted zone was required to travel at a relatively fast rate to maintain a continuous and well-defined germination at the solid-liquid interface. The resulting solidification stresses establishes a dislocation network at a thermodynamic metastable equilibrium at room temperature. These stresses may be responsible for the dilatation anomalies of the initial cycles in accordance with the observations of Rosenholtz *et al.*[13] But the preliminary heat treatment at 450 °C should, to a large extent, anneal out these stresses. We prefer to base our interpretations on the easy condensation of vacancies into loops as observed by Poirier *et al.*,[14] and recently by Hillairet *et al.*,[15] from their quenching experiments. It is, therefore, not impossible to find in Mg a process analogous to that observed by Baudelet and Champier[16] in Al. During solidification, some vacancies do not go to sinks but condense into small imperfect loops in metastable equilibrium at room temperature. The preliminary annealing at 450 °C does not eliminate these faulted loops definitely but allows them to develop in the cooling process. During the first heating cycles, these loops act as preferential sinks for vacancies until their complete disappearance, while the Frank network of dislocations are the most efficient vacancy sources. To verify this point, the relative increase of sites corresponding to the first heating cycle was calculated using Eq. (3) and shown on column C' of Table II. (For this calculation, the lattice dilatations at low temperatures were adjusted to the macroscopic dilatations as described above.) It is impossible to adjust C' to a single relation of the type

$$C' = e^{S'_f/k} e^{-E'_f/kT} .$$

An adjustment using only the temperatures lower than 300 °C gives an apparent formation energy $E'_f \simeq 0.32 \pm 0.05$ eV, while near the melting point, one obtains $E'_f \simeq 0.53$ eV. If it is supposed that the sites created at low temperatures are due to the faulted loops, the apparent formation energy must be

$$E'_f \simeq E_f - \gamma s ,$$

where γ is the energy of the stacking fault and s the site area (the variation of the line energy is neglected). If E_f is taken equal to 0.58 eV, as obtained above, and $E'_f = 0.32 \pm 0.05$ eV, then $\gamma = 250 \pm 50$ erg/cm^2 which is compatible with the estimate of Hillairet *et al.*,[15] and the measurements of Harris and Masters.[17] Tables II and III show that the "low-temperature" process favors the direction parallel to the c axis, indicating a maximum density of faulted loops on the basal plane in accordance with the observations of Hillairet *et al.*[15] on materials of equivalent purity.

During the cooling that follows the first rise in temperature, some vacancies condense into new loops which develop progressively until a practically stable dislocation network is established.[16] This stable state requires several heating-cooling cycles whose number is least for the basal-plane directions in accordance with the idea that the structural defects evolve much faster in the prismatic planes. The dislocations formed by the point defects created by the first heating cycles would be responsible for the residual dilatation observed.

B. Formation Energy and Entropy

Work on the dilatation of Mg is very limited. Goens *et al.*[18] give 26.96×10^{-6} and 28.3×10^{-6} for the macroscopic-dilatation coefficients on the basal plane and along the c-axis directions, respectively. The values fit very well with our results, i.e., 26.7×10^{-6} and $28.4\times10^{-6}(\pm 0.2\times10^{-6})$. Raynor and Hume-Rothery[19] reported lattice-dilation values which agree with the present study up to 450 °C; at higher temperatures, their values are always greater than ours.

Experimental determinations of vacancy-formation parameters in Mg are also rare. Mairy *et al.*[20] measured the resistance of Mg wires in thermal

equilibrium and deducing the defect concentration from the difference between the variations at low temperatures and the extrapolated law, found the formation energy to be between 0.78 and 0.81 eV. Beevers[21] measured the resistivity after quenching to − 80 °C and obtained 0.89 eV for the formation energy. Recently, Hillairet *et al.*[15] also measured the resistivity after quenching and gave the values 0.80–0.93 eV, depending upon the conditions of the quench. There is not any direct determination of the formation entropy in the literature. One finds one measurement of self-diffusion energy by Schewmon[22] giving 1.40 and 1.39 eV, respectively, for the basal plane and along the c axis and some results concerning the migration energy of vacancies: 0.5–0.6 eV by Levy *et al.*[23] (resistivity after quenching and annealing), 0.40–0.45 eV by Nicoud[24] (resistivity after irradiation), and 0.52 eV by Beevers (resistivity after cold deformation).

A comparison between the formation energy obtained in the present study (0.58 eV) with those cited above (0.78–0.93 eV) shows a difference too large to be solely due to measurement errors. A critical examination of the experimental conditions allows the following remarks.

1. *Divacancy and Impurity Effects*

It is well known that the apparent formation energy of single vacancies is lower than its real value because the formation of divacancies at high temperatures and the existence of vacancy-impurity interactions. However, calculations show that the presence of divacancies in the neighborhood of the melting point cannot modify the present determinations to a quantity greater than 1%, even if high values for the binding energy are used (0.30–0.35 eV).

Recently, Hillairet *et al.*[15] ascribed the large difference in quenched resistivity between ultrapure Mg (1 ppm) and less pure Mg (30 ppm) to a high vacancy-impurity binding energy. If this is so, the measured vacancy concentration in the presence of impurities is given by

$$C = A\, e^{-E_f/kT}\,(1 - Zi + Zi\, e^{E_L/kT}) ,$$

where Z is the coordination number of the metal (12 for the present case), i is the impurity concentration, and E_L is the vacancy-impurity binding energy.

Using this new definition for the experimental values, C in the calculations, in which the impurity content was varied between 100 and 500 ppm and the binding energy between 0 and 0.5 eV, the computer-obtained values show that the correlation coefficient between the experimental and the optimal calculated values is least for small i and E_L ($i \sim 100$ ppm and $0 \leq E_L \leq 0.2$ eV) even for the smallest confidence range for A and E_f. This appears in Table IV and eliminates the impurity effect in the present study.

2. *Imperfect Loops as Vacancy Sources*

The lowering of the formation energy of vacancies when the imperfect loops are the sources was already invoked above and it was seen that a stacking-fault energy of about 250–300 erg/cm^2 corresponds in this case to an energy-of-formation decrease of 0.30 eV, which is exactly the order of magnitude and sign of the difference between our results and those cited in the literature. However, it seems difficult to make this interpretation for at least two reasons: (i) After several slow anneals by raising the temperature up to the neighborhood of the melting point, it seems very improbable that faulted loops would remain in the specimens. (ii) In the resistivity measurements in equilibrium[20] and after quenching,[15,21] the imperfect loops would also create vacancies resulting in a formation energy for vacancies decreased by the same order of magnitude.

TABLE IV. Impurity effect on the vacancy-formation energy.

i(ppm)	E_L (eV)	E_f (eV)	A	ρ^2	$10^5\, C_f$
0	···	0.58 ± 0.012	1.049 ± 0.450	0.99954	71.9
100	0.2	0.58 ± 0.019	1.033 ± 0.739	0.99954	70.9
100	0.3	0.60 ± 0.021	1.284 ± 0.891	0.99949	68.4
100	0.4	0.66 ± 0.026	2.426 ± 1.853	0.99933	60.9
100	0.5	0.82 ± 0.029	13.064 ± 9.637	0.99931	44.0
300	0.2	0.59 ± 0.020	1.143 ± 0.788	0.99953	69.1
300	0.3	0.63 ± 0.022	1.706 ± 1.222	0.99947	62.4
300	0.4	0.75 ± 0.026	5.753 ± 4.183	0.99947	46.7
300	0.5	0.93 ± 0.030	29.025 ± 18.020	?	?
500	0.2	0.59 ± 0.020	1.110 ± 0.823	0.99953	67.3
500	0.3	0.65 ± 0.022	2.01 ± 1.518	0.99948	57.4
500	0.4	0.79 ± 0.024	7.667 ± 5.863	0.99929	37.9
500	0.5	0.97 ± 0.017	33.287 ± 23.801	0.99915	17.2

3. *Resistivity-Measurement Results*

The three studies preceding the present work are resistivity measurements on wire or ribbon specimens formed by drawing or rolling. It must be noted that in forming the specimens, a texture is produced in the specimen wherein the basal plane forms an angle of about 10° with the drawing axis, and this texture remains after annealing.[25] Considering that the material is anisotropic, that the process of defect formation depends on crystallographic orientation, and that the quenched clusters have anisotropic structures,[15] it seems difficult to establish a simple relation between the physical measurements on this texture (equilibrium and quenched resistivity) and the vacancy concentration in the specimen at a given temperature.

Also, and this is very important, it seems that the three cited studies could not have been made on correctly stabilized specimens. The present work shows that several cycles of slow temperature rise and cooling are required for the stabilization of the dislocation network which is formed by the small loops created during the quench (or slow cooling of a few degrees per second) by the condensation of vacancies. Beevers,[21] Mairy,[20] and Hillairet[15] annealed by maintaining their specimens for a certain time at a given temperature of the order of 450 or 500 °C, thus putting their "no vacancy" reference in a state similar to that of our specimens during the first or second heating cycles. To verify this point, we determined the "point-defect concentration" using only the measurements for the first heating cycles by finding the difference between the low-temperature (below 400 °C) dilatation curve extrapolated to the melting point and the real "high-temperature" curve. The mathematical treatment already described gives a "formation energy" equal to 0.80 eV for an apparent vacancy concentration of 3.16×10^{-4} in the neighborhood of the melting point. As it was seen before, a comparison with the lattice dilatations indicates that the macroscopic-dilatation curves of the first cycles are not characteristic of the reversible formation of vacancies.

It is known that quenches cannot be fast enough to retain all the vacancies. Therefore, even when the processes of formation and elimination of defects are isotropic, one entertains a few doubts on the results obtained from measurements after quenching.

The case of Mg is still more disturbing since a single type of defect, that of vacancies, seems to exist, but these vacancies are divided into two families: those which appear (or disappear) easily on the prismatic planes and those which are formed and eliminated with more difficulty on the basal planes. Logically, the vacancies that disappear during the quench are those of the first family and therefore the resistivity measurements are highly affected by second family. Making the exaggerated supposition that only the latter remain, the corresponding apparent formation energy can be estimated from the dilatation measurements obtained here for the direction parallel to the c axis. One obtains 0.96 eV.

These two remarks tend to prove that the values of 0.78–0.93 eV are really too high; the experimental methods used must be responsible for the systematic errors.

4. *Correlations between E_f and Other Physical Quantities*

Usually the self-diffusion energy is taken to be the sum of the formation and migration energy of a vacancy. For Mg, the rare estimations of the self-diffusion energy give $1.3 \leq E_A \leq 1.4$ eV, while the migration energy is quoted as $0.4 \leq E_m \leq 0.7$ eV. If this rule is accepted, it is deduced that the formation energy must be between 0.6 and 1 eV. Another rule which is also very often cited, $E_f = \frac{1}{2}E_A$, would place the formation energy in the range $0.65 \leq E_f \leq 0.70$ eV. In both cases, the value obtained here, $E_f = 0.58$ eV, is outside the permissible range. Meanwhile, one can ask if the measured values E_A are not systematically increased by a contribution of the migration entropy. The latter is a function of temperature since the creation of vacancies by atom movement has an anisotropy which, initially appreciable, decreases near the melting point. It seems, therefore, logical to write $S_A = a + b/T$. The term b/T would then be involved in the determination of E_A by the slope method. It must also be noted that the two cited rules, although well verified for fcc metals, do not seem to hold for hcp metals. For cadmium, for instance,

$$0.31 \leq E_f \leq 0.40 \text{ eV},$$

$$0.23 \leq E_m \leq 0.25 \text{ eV}.$$

The sum $0.54 \leq E_f + E_m \leq 0.65$ eV is much lower than $0.76 \leq E_A \leq 0.89$ eV, while the rule $E_f = \frac{1}{2}E_A$ is almost satisfied.

Table V summarizes experimental quantities which may allow certain empirical correlations between the vacancy formation energy E_f, the melting point temperature T_f, the cohesion energy E_c, and the Debye temperature θ_D. All the elements shown have close-packed structure; the E_f values are those already cited above or those reported by Quéré[26]; the T_f, θ_D, and E_c values were taken from Gschneider.[27] The relation $E_f = K m a^2 \theta_D^2$, where m is the atomic mass of the element and a the lattice parameter, was established by Glyde[28] for close-packed structures. With Table V, the following remarks can be said: (i) $0.20 \leq E_f/E_c \leq 0.37$;

TABLE V. Correlations between the vacancy-formation energy and some physical properties.

Metal	E_f (eV)	T_f (°K)	Θ_D (°K)	E_c (eV)	E_f/T_f (10^{-3} eV °K^{-1})	E_f/E_c	$K=E_f/ma^2\Theta_D^2$
Al	0.76	933	403	3.34	0.81	0.23	1.06
Cu	1.00	1356	332	3.52	0.74	0.28	1.09
Ag	1.06	1234	213	2.97	0.86	0.36	1.29
Au	0.95	1336	160	3.81	0.71	0.25	1.13
Ni	1.35	1726	443	4.45	0.78	0.33	0.95
Pt	1.20	2042	229	5.85	0.59	0.20	0.76
Cd	0.31	594	160	1.17	0.52	0.26	1.21
	0.40				0.67	0.34	1.56
Zn	0.31	692	231	1.35	0.45	0.23	1.25
	0.50				0.72	0.37	2.02
Co	1.25	1765	446	4.42	0.71	0.28	1.70
Mg	?	923	363	1.55			K 0.33

if Mg satisfies this correlation, E_f can only be between 0.31 and 0.59 eV. (ii) $0.45\times10^{-3} \leq E_f/T_f \leq 0.86\times10^{-3}$; this gives for Mg a magnitude within the range 0.41–0.79 eV for E_f. (iii) $0.76 \leq K \leq 2.02$; here E_f is found to be between 0.25 and 0.65 eV for Mg. It seems, therefore, that, despite the disagreement with preceding studies, our value of 0.58 eV for the vacancy-formation energy in Mg is perfectly acceptable and we have seen how the resistivity measurements can have systematic errors.

The entropy term seems to be small since one usually expects values S_f/k in the order of unity.[29] However, if one considers that the atomic mass of Mg is three times smaller than that of Zn and five times lower than that of Cd, it would seem that the vacancy in Mg is a small mass defect. It is seen also that a vacancy in Mg is a defect of force constants much smaller than a vacancy in Zn or in Cd whose interatomic force constants are about three times larger[30] (11.84, 30.82, 27.52×10^{-3} dyne/cm, respectively). Logically, the modes vibration of the lattice must be only slightly perturbed and the formation entropy must be much smaller than for Cd ($S_f/k=0.7$, Feder and Novick) or for Zn ($S_f/k=1.6$, Gerstriken and Slyusar[31]).

In conclusion, it can be said that, although results are obtained with the use of so much mathematical treatment in the case of anisotropic materials, a direct comparison of the relative variations of lattice and macroscopic volume as a function of temperature is the most desirable method for the estimation of point-defect concentration. Also, the values proposed for the vacancy-formation energy in magnesium preceding the present work must be reexamined.

[1]J. D. Eshelby, J. Appl. Phys. 25, 255 (1954).

[2]R. O. Simmons and R. W. Balluffi, Phys. Rev. 117, 52 (1960).

[3]R. O. Simmons and R. W. Balluffi, Phys. Rev. 119, 600 (1960).

[4]R. O. Simmons and R. W. Balluffi, Phys. Rev. 125, 862 (1962).

[5]R. O. Simmons and R. W. Balluffi, Phys. Rev. 129, 1533 (1963).

[6]R. Feder and A. S. Nowick, Phil. Mag. 15, 805 (1967).

[7]R. Feder and H. P. Charbnau, Phys. Rev. 149, 464 (1966).

[8]R. Feder, A. S. Nowick, and H. P. Charbnau, Bull. Am. Phys. Soc. 12, 388 (1967).

[9]G. Bianchi, thesis, Nancy, 1968 (unpublished).

[10]D. Mallējac, thesis, Nancy, 1970 (unpublished).

[11]H. M. Gilder and G. N. Wallmark, Phys. Rev. 182, 771, (1969).

[12]A. C. Damask and G. J. Dienes, *Point Defect in Metals* (Gordon and Breach, New York, 1963).

[13]J. L. Rosenholtz and D. T. Sonith, J. Appl. Phys. 21, 396 (1950).

[14]J. P. Poirier, J. Antolin, and J. M. Dupouy, J. Phys. (Paris) 27, 98 (1966).

[15]J. Hillairet, C. Mairy, J. Expinasse, and V. Levy (private communication).

[16]B. Baudelet and G. Champier, J. Phys. 30, 999 (1969).

[17]J. E. Harris and B. C. Masters, Proc. Roy. Soc. (London) A292, 240 (1966).

[18]E. Goens and E. Schmid, Z. Physik 37, 385 (1936).

[19]G. V. Raynor and W. Hume Rothery, J. Inst. Metals 65, 379 (1939).

[20]C. Mairy, J. Hillairet, and D. Schumacher, Acta. Met. 15, 1258 (1967).

[21]C. J. Beevers, Acta. Met. 11, 1029 (1963).

[22]P. G. Schewmon, Trans. AIME 206, 918 (1956).

[23]V. Levy, J. Hillairet, D. Schumacher, G. Revel, and T. Chaudron, in Proceedings of the International Conference on Vacancies and Interstices in Metals, Jülich, W. Germany, 1968 (unpublished).

[24]J. C. Nicoud (private communication).
[25]J. Mianney, thesis, University of Paris, 1969 (private communication).
[26]Y. Quéré, *Defauts Ponctuels dans les métaux*, edited (Masson et Cie., Paris, 1967).
[27]K. A. Gschneider, Solid State Phys. 16, 344 (1964).
[28]H. R. Glyde, J. Phys. Chem. Solids 28, 2061 (1967).
[29]L. Dobrzynski (private communication).
[30]G. Toussaint, in *Proceedings of the International Conference on Lattice Dynamics*, Copenhagen, 1963, edited by R. F. Wallis (Pergamon, Oxford, 1965).
[31]S. D. Gertsriken and B. F. Slyusar, Ukr. Fiz. Zh. 4, 137 (1959).

PHYSICAL REVIEW B VOLUME 2, NUMBER 8 15 OCTOBER 1970

New Version of the Modified Augmented-Plane-Wave Method*

H. Bross, G. Bohn, G. Meister, W. Schubö, and H. Stöhr
Sektion Physik, University of Munich, Germany
Received 5 September 1969

A method is presented to calculate electronic band structures for a general one-electron potential. Both the wave functions and their gradients are continuous everywhere in the crystal. As a test, calculations for paramagnetic Ni, Cu, and Al by Hanus, Burdick, and Segall, respectively, were repeated, using their muffin-tin potentials.

I. INTRODUCTION

Among the different methods to calculate the band structure of solids, the augmented-plane-wave (APW) method proposed by Slater[1,2] has proved particularly useful. It is based on the fact that the crystal potentials near an atomic site are approximately spherically symmetric. Therefore, the crystal will be divided into several parts by constructing a sphere (radius r_i) about each atomic site. The wave function is expanded inside each sphere in terms of radial functions multiplied by spherical harmonics; in the region between the spheres the wave function is expanded in a Fourier series of plane waves. Across the surfaces of the spheres, the APW method in its original form makes the partial waves continuous, however, for the lower values of the azimuthal quantum number l only. Usually all the calculations using the APW method are based on a muffin-tin potential, which is spherically symmetric inside the atomic spheres and has a constant value outside.

Within the one-electron approximation, several improvements of the APW method are desirable: (i) exact continuity of both the wave functions and their first derivatives on the surfaces of the APW spheres (this is a necessary requirement if the wave functions are to be used to calculate matrix elements, in particular, those of the momentum operator and functions thereof), (ii) generalization of the method to allow for non-muffin-tin potentials (this step should be done if the band structure is calculated in a self-consistent manner), (iii) orthogonality of the wave functions of the valence electrons to the wave functions of the core electrons. Preferably the core electrons should be described by Bloch functions also.

In addition, one would like to have a formalism which can be handled on a computer using standard techniques of numerical analysis.

Different modifications of the APW method[3-10] have been proposed with the above-mentioned goals. The version previously proposed by one of the present authors[5,8,9] incorporates the first requirement. Further, it allows for a nonconstant potential in the plane-wave region as do the formulations of Leigh,[3] Schlosser and Marcus,[4] and De Cicco.[6] General potentials have been studied by Marcus[7] and others.[8-10] In the 1937 formulation of the APW method, the wave functions of the valence electrons are orthogonal to those of the core states if the latter are also determined by the APW method. The aim of this paper is to describe a new version of the modified-augmented-plane-wave method (MAPW) which produces wave functions of the valence electrons orthogonal to the wave functions of the core electrons and which is especially suited for computers. Applications to paramagnetic Ni, Cu, and Al are reported with the special view towards comparing the results with earlier calculations.[11-13]

II. DESCRIPTION AND DISCUSSION OF METHOD

A. MAPW Trial Functions

As in the original APW method, we approximately solve the one-electron Schrödinger equation by the